



Supplement of

Distribution and sea-to-air exchange of carbon monoxide in surface microlayer and subsurface seawater in the eastern marginal seas of China

Lin Yang et al.

Correspondence to: Jing Zhang (zhangjouc@ouc.edu.cn) and Gui-Peng Yang (gpyang@mail.ouc.edu.cn)

The copyright of individual parts of the supplement might differ from the article licence.

Supplementary Information

S1. Analytical measurements

S1.1 Determination of the CDOM spectral absorption coefficient

Absorption spectra were determined using a UV-visible spectrophotometer (UV-2550 bi-channel; Shimadzu, Tokyo, Japan) equipped with two 10 cm path-length quartz cuvettes. Sample absorbance was automatically corrected for the absorbance of Milli-Q water. Absorbance scans ranged from 200 to 800 nm, with a spectral resolution of 1 nm. The absorption coefficient of CDOM was calculated according to equation (S1):

$$a(\lambda) = 2.303 A(\lambda) / l \quad (\text{S1})$$

where, $A(\lambda)$ is the absorbance at wavelength λ ; and l is the path length of the quartz cuvette in meters.

The spectral slope of the CDOM absorption curve (S) was calculated according to a non-linear regression over the 275–500 nm wavelength range, according to:

$$\alpha(\lambda) = \alpha(\lambda_0)\exp[S(\lambda_0 - \lambda)] + K \quad (\text{S2})$$

where, $\alpha(\lambda)$ is the absorption coefficient at wavelength λ ; $\alpha(\lambda_0)$ is the absorption at the reference wavelength λ_0 of 440 nm; S is the spectral slope; and K is a background parameter that accounts for baseline shifts or attenuation due to factors other than CDOM. S was measured in the wavelength ranges of 275–295 nm ($S_{275-295}$, nm^{-1}) and 350–400 nm ($S_{350-400}$, nm^{-1}). $S_{275-295}$ is used to characterize DOM, with low values generally indicative of high-molecular-weight DOM that are linked to photochemical modification (Helms et al., 2008; Ortega-Retuerta et al., 2009). The spectral slope ratio (S_R) was defined as the ratio of the two spectral slopes, $S_{275-295}$ to $S_{350-400}$. S_R is also a sensitive indicator of photochemically induced changes in the molecular weight within the CDOM pool, with increases in S_R suggesting stronger photodegradation (Ortega-Retuerta et al., 2009; Spencer et al., 2009). The absorption coefficient at 254 nm ($a(254)$), the absorption of light at 254 nm per unit of carbon, was used to quantify CDOM abundance. The specific UV absorbance (SUVA_{254}) can be

25 used to measure aromaticity (Weishaar et al., 2003; Massicotte et al., 2017) and molecular weight
26 (Chowdhury, 2013) of DOM, with higher values generally indicative of higher aromaticity.

27 *SI.2 EEMs and determination of the CDOM fluorescence index*

28 EEMs fluorescence spectra were obtained using a F-4500 fluorescence spectrophotometer with
29 a 1 cm quartz cuvette (Shimadzu) (Hoge et al., 1993). The emission spectra were scanned every 5
30 nm from 250 nm to 550 nm, and at the excitation wavelengths between 200–400 nm at 5 nm
31 intervals, with 5 nm slit widths for the excitation and emission modes. The FL Toolbox, which was
32 developed by Wade Sheldon (University of Georgia) for MATLAB, was used to remove the
33 Rayleigh and Raman scattering peaks using the Delaunay triangulation method (Zepp et al., 2004).
34 The fluorescence intensities of the samples were corrected with Milli-Q water blank EEMs and then
35 normalized to the water Raman integrated area maximum fluorescence intensities (Ex/Em = 350
36 nm/365–430 nm, 5 nm bandpass) (Singh et al., 2010). Parallel factor analysis (PARAFAC)
37 statistically decomposes the all measured EEMs of CDOM samples into individual trilinear terms
38 and a residual array (Kowalczyk et al., 2010):

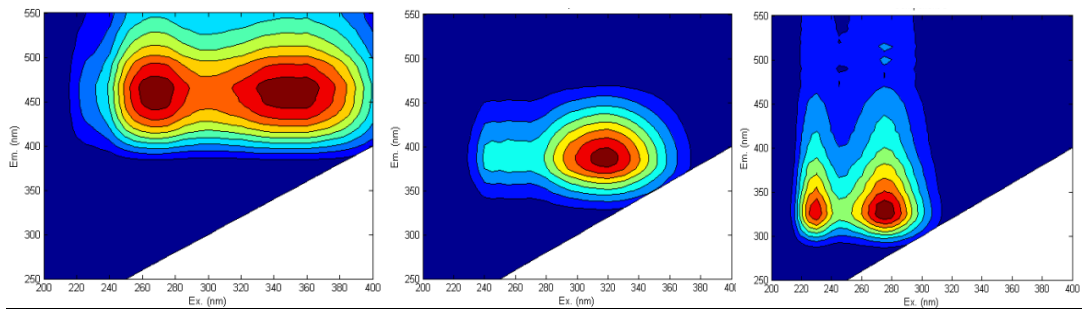
$$39 \quad X_{ijk} = \sum_{n=1}^F a_{in} b_{jn} c_{kn} + \varepsilon_{ijk} \quad (S3)$$

40 where X_{ijk} is the fluorescence intensity of the i th sample at the k th excitation and j th emission
41 wavelengths; a_{in} is directly proportional to the concentration (scores) of the n th fluorophore in the
42 i th sample; b_{jn} and c_{kn} are the estimates of the emission and excitation spectra (loadings) of the n th
43 fluorophore at wavelengths j and k , respectively; F is the number of components (fluorophores);
44 and ε_{ijk} represents the unexplained variability of the model (Singh et al., 2010). Split-half analysis
45 validation was used to determine the number of fluorescent components. The fluorescence intensity
46 of each fluorescent component was evaluated (Fig. S1, Table S1). Raman units (RU) (Stedmon et
47 al., 2007; Singh et al., 2010) were used as the units for the Raman peak areas of water when the
48 excitation wavelength of 350 nm was used for correction. EEMs were modeled using PARAFAC in
49 MATLAB 7.5 with the DOMFluor toolbox (Stedmon and Bro, 2008).

50 *SI.3 Determination of DOC, chlorophyll-a, heterotrophic bacterial abundance, dissolved oxygen,* 51 *and other parameters*

52 Concentrations of DOC were determined using the Shimadzu TOC-V_{CPH} total organic carbon

53 analyzer with an injection volume of 80 μ L. The accuracy of the test was ensured by measuring a
54 deep seawater reference (Hansell Laboratory, University of Miami) every 10 samples. For Chl-a
55 analysis, 200 mL subsamples were filtered through 0.7 μ m GF/F filters (Whatman, U.S.A.), which
56 were then stored in the dark at 20 °C until analysis. The Chl-a was extracted in 90% acetone and
57 centrifuged for 10 min at 4 °C before being measured with a fluorescence spectrophotometer (7200-
58 000, Turner Designs, CA) according to the method from Parsons et al. (1984). Dissolved oxygen
59 (DO) was determined by iodination using the Winkler titration method (Carpenter, 1964), the
60 endpoint was determined using starch as a visual indicator.



61

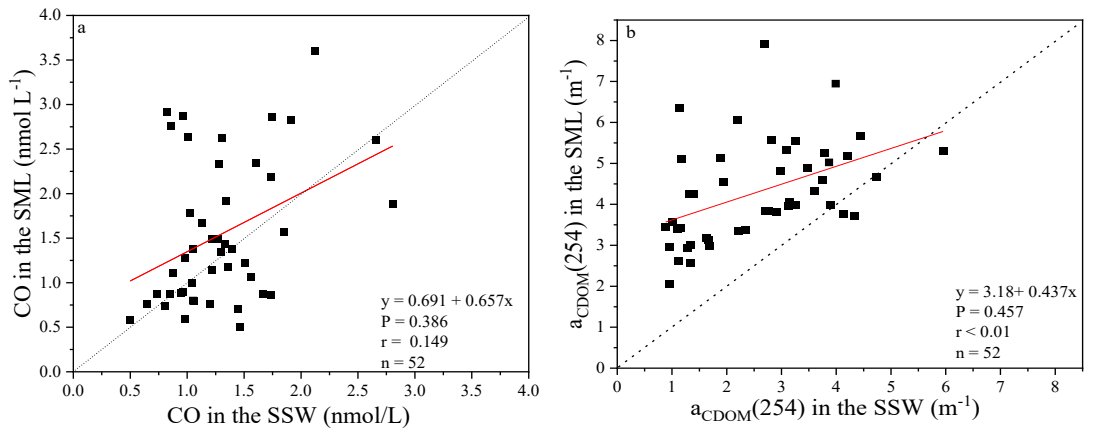
62

63

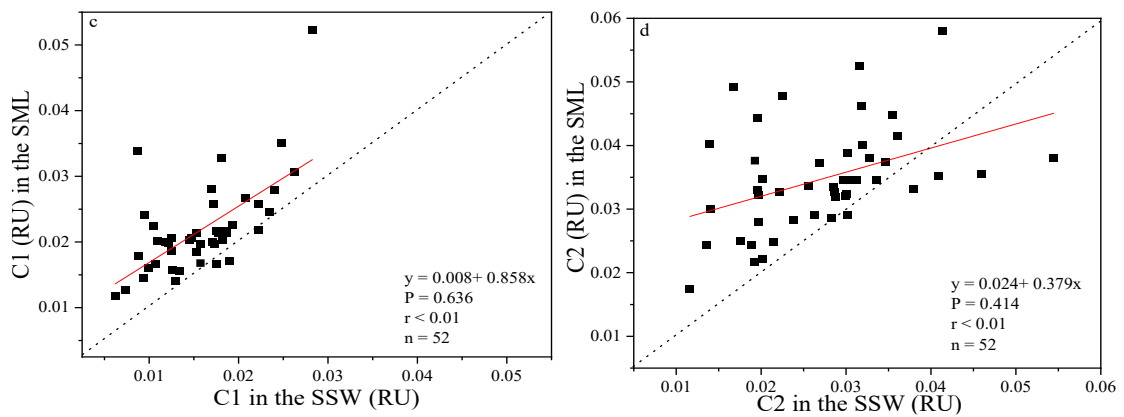
64

65

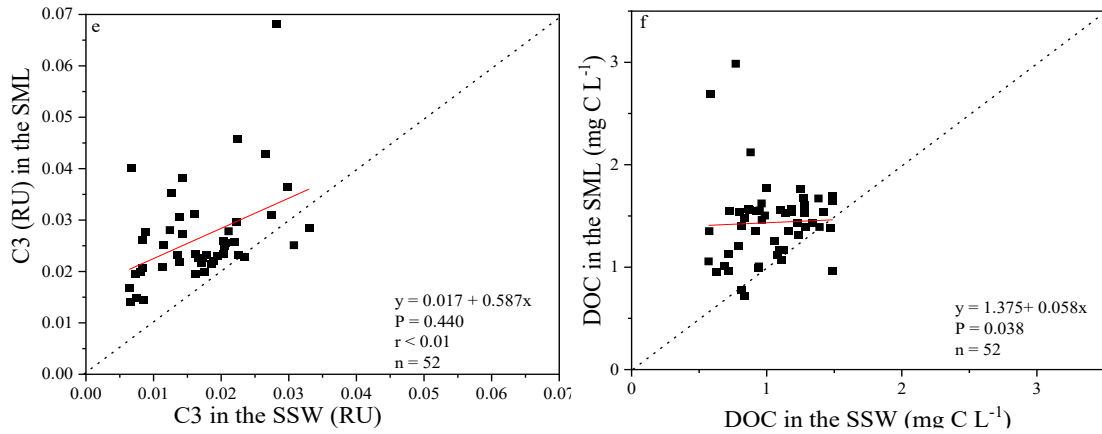
Fig. S1. Representative fluorescence excitation-emission matrix spectra (EEM) contours from samples in the ECS and the YS during winter. The fluorescence intensities were quantified using Raman units (nm^{-1}).



66



67



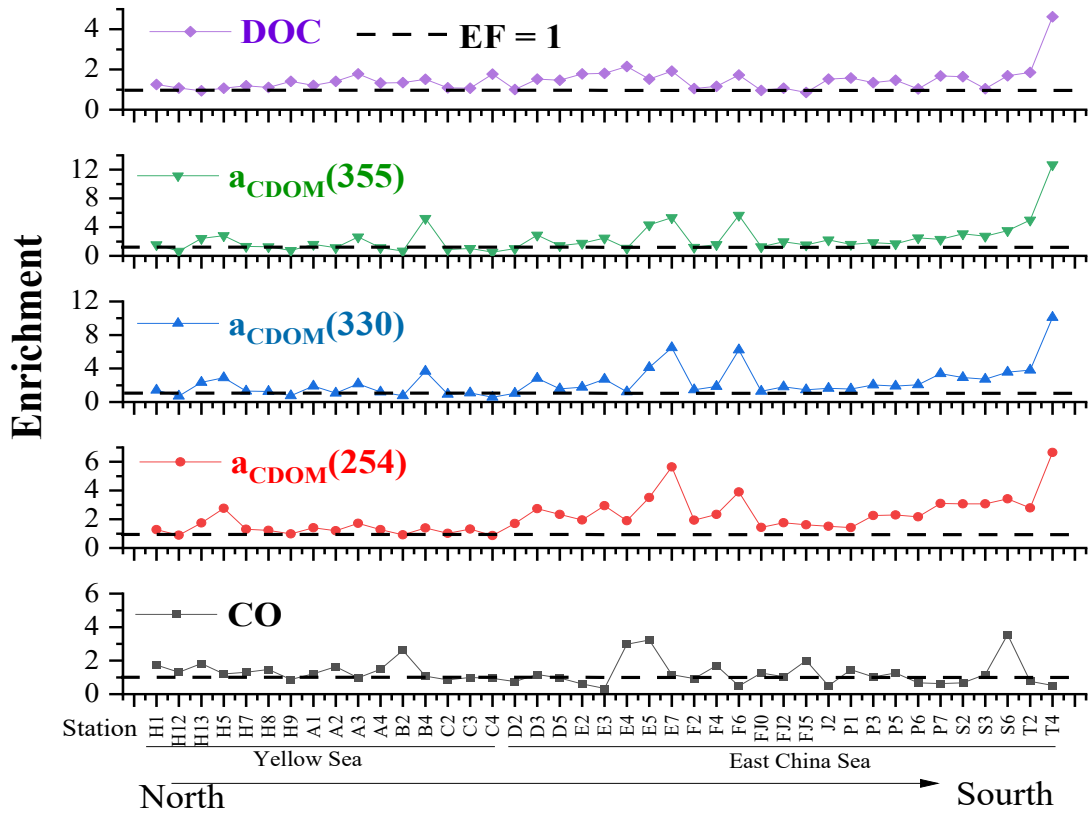
68

69

70

71

Fig. S2. Correlations between the microlayer CO, CDOM, DOC, and three fluorescence components, as well as their sub-surface water concentrations in winter. The dashed lines correspond to the 1:1 lines, and the full lines are the regression models.



72

73

74

75

76

Fig. S3. EFs of CDOM absorption, DOC, and CO in the SML at different stations.

77 Table S1. Location, local time, depth, temperature, salinity, wind speed and net radiation conditions

78 of SML and SSW water sampling.

Station	Time	Longitude	Latitude	Depth (m)	Temperature (°C)	Salinity	Wind speed (m/s)	Net radiation
A1	5:25	121.25	35.98	34	8.29	32.18	5.91	-103.9
A2	9:45	122.15	35.98	43	10.12	31.97	1.53	147.9
A3	14:16	123.05	35.98	69	11.27	32.25	2.78	50.6
A4	19:01	123.97	35.98	74	10.25	32.25	3.25	-52.3
B1	22:35	120.51	35.00	27	10.15	31.72	3.15	-77.3
B2	18:07	121.35	35.00	33	11.11	31.83	3.40	-55.6
B3	13:34	122.20	35.00	52	11.77	32.09	7.67	187.3
B4	8:42	123.06	35.00	67	11.51	32.35	8.82	32.3
B5	2:22	123.98	35.00	78	11.09	32.41	10.05	-42.4
C1	5:02	121.25	34.00	12	8.69	31.10	7.29	-86.8
C2	9:33	122.14	34.00	17	10.93	31.66	4.27	85.6
C3	14:19	123.05	34.00	66	12.30	32.42	3.67	2.7
C4	19:11	124.00	34.00	75	12.67	32.83	7.53	-38.6
D1	17:11	122.49	31.36	18	10.90	31.22	8.66	-15.4
D2	19:09	122.49	31.60	22	10.15	31.13	6.91	-23.7
D3	22:50	122.99	31.90	32	14.01	32.94	5.32	-28.1
D4	3:19	123.50	32.15	35	13.46	32.44	6.84	-27.4
D5	6:05	124.00	32.45	36	13.43	32.28	7.92	-32.9
E1	1:58	122.31	29.36	12	13.64	28.85	4.03	-82.8
E2	22:22	122.61	29.11	48	16.56	33.30	6.53	-15.2
E3	18:17	123.01	28.83	63	18.40	34.01	2.08	-20.5
E4	13:34	123.57	28.48	70	18.99	34.22	3.42	288.0
E5	8:05	124.25	27.95	96	19.35	34.49	3.53	94.7
E6	2:05	125.00	27.45	97	20.77	34.53	4.25	-80.5
E7	18:19	125.80	26.87	1136	23.75	34.62	2.18	-91.1
F2	20:37	126.33	31.89	88	18.15	34.30	8.49	-15.4
F3	17:14	126.50	31.30	85	18.05	34.23	8.60	-23.4
F4	12:43	126.85	30.50	91	19.33	34.34	7.80	417.9
F5	7:31	127.25	29.65	123	20.22	34.51	5.77	94.1
F6	1:39	127.60	28.80	1003	23.43	34.45	6.84	-89.4
FJ0	15:01	122.80	31.33	52	14.86	32.65	7.39	-19.9
FJ1	13:37	123.50	31.33	46	16.66	33.95	12.00	183.4
FJ2	7:48	124.50	31.34	50	15.49	32.90	11.19	51.8
FJ3	3:38	125.31	31.32	54	14.66	32.39	7.27	-12.4
FJ5	14:31	122.60	30.10	24	13.69	29.03	8.23	18.8
H1	9:55	122.74	36.97	28	6.35	31.99	9.80	165.8
H10	21:25	123.00	38.75	51	7.36	32.20	3.11	-104.1

H11	2:04	123.80	38.75	51	7.75	32.18	5.58	-62.3
H12	7:15	123.97	39.50	19	2.09	30.79	5.09	-96.3
H13	11:11	123.21	39.29	31	4.77	31.92	4.79	226.7
H2	6:00	123.38	37.00	68	9.16	32.14	9.12	-20.3
H3	2:31	123.97	37.00	74	9.62	32.25	7.94	-85.5
H4	19:04	123.96	38.00	72	8.84	32.20	6.50	-110.0
H5	23:33	123.00	38.00	55	7.90	32.23	4.75	-111.8
H6	4:19	122.05	38.00	46	7.41	32.22	8.39	-107.4
H7	8:47	121.16	38.00	17	6.48	32.26	4.60	25.7
H8	11:12	121.16	38.36	47	7.14	32.24	1.48	236.3
H9	16:37	122.08	38.75	46	4.67	32.16	0.68	-94.6
J1	20:48	122.01	33.00	11	8.64	31.54	4.51	-17.4
J2	15:21	123.01	32.96	28	12.35	31.68	6.82	-14.2
J3	9:58	123.99	33.00	45	13.22	32.42	6.25	71.0
P1	12:15	122.72	30.96	19	13.96	30.61	3.59	22.9
P2	9:53	123.01	30.87	47	15.76	33.04	2.90	14.1
P3	21:31	123.75	30.37	53	17.48	33.96	6.98	-87.4
P4	2:40	124.55	29.85	62	17.61	33.88	8.52	-81.8
P5	8:48	125.39	29.27	87	18.97	34.19	7.49	266.0
P6	14:36	126.15	28.70	121	20.62	34.51	7.17	118.7
P7	20:15	127.00	28.15	899	23.31	34.66	7.32	-75.5
S1	9:55	121.47	27.85	22	14.01	29.78	7.81	222.9
S2	13:05	121.63	27.58	44	17.83	33.90	8.93	266.6
S3	16:37	122.00	27.33	83	19.52	34.34	5.87	-53.6
S4	12:08	122.75	27.15	104	20.42	34.51	5.46	30.7
S5	2:44	123.36	26.65	138	21.05	34.35	4.25	-33.9
S6	8:05	124.2	26.54	140	22.98	34.43	4.80	162.0
T1	0:56	120.51	26.84	22	14.59	29.61	8.69	-33.2
T2	21:12	120.92	26.61	59	17.88	33.15	3.04	-26.6
T3	17:22	121.35	26.30	75	20.12	33.58	4.02	-12.8
T4	13:31	121.77	26.00	117	19.62	34.07	5.98	17.9
T5	6:03	122.67	25.48	659	19.75	34.43	9.44	-9.1

Table S2. Shapiro-Wilk test for normality of the full datasets; the test statistic (W), degrees of freedom (df) and probability value (p) are listed for each.

Shapiro-Wilk	[CO] _{ssw}	[CO] _{sml}	a _{CDOM} (254) in the SSW	a _{CDOM} (254) in the SML	DOC in the SSW	DOC in the SML
w	0.918	0.901	0.928	0.615	0.978	0.396
df	69	43	69	53	69	53
p	< 0.001	0.001	< 0.001	< 0.001	0.258	< 0.001

Table S3. Spectral characteristics of the three fluorescent components identified by the PARAFAC model in this study, compared with those previously identified.

Component	E _x : E _m	Tradition peak Coble (2007)	Fluorescence type	Comparison with other studies using PARAFAC
C1	275/335	Peak T:275/340	Tryptophan-like	Tryptophan-like C5: 275/330 (Zhu et al., 2017) Tryptophan protein-like C5: 275/325 (Chari et al., 2012) Tryptophan-like C4: 275/340 (Guo et al., 2014)
C2	350/455	Peak C:320-360/420-460	Terrestrial humic-like	Humic-like C1: 330/425 (Zhu et al., 2017)
C3	320/390	Peak M:290-310/370-410	Marine humic-like	Marine humic-like C3: 250(310)/400 (Kowalczyk et al., 2010) Marine humic-like C1: < 250(310)/416 (Williams et al., 2010) Humic-like C2: 250/420 and C3: 250(310)/400 (Kowalczyk et al., 2010)

Table S4. Production rate and biological consumption rate of CO in the sea surface microlayer and subsurface water of the eastern marginal seas of China and its sea-to-air flux.

Station	Time	Temperature (°C)	Salinity	SML		SSW		Wind speed (m s ⁻¹)	Flux in the SML (nmol L ⁻¹ h ⁻¹)	Flux in the SSW (nmol L ⁻¹ h ⁻¹)	[CO] _{sur} (nmol L ⁻¹)
				k _{bio} (nmol L ⁻¹ h ⁻¹)	k _{photo} (nmol L ⁻¹ h ⁻¹)	k _{bio} (nmol L ⁻¹ h ⁻¹)	k _{photo} (nmol L ⁻¹ h ⁻¹)				
A1	5:25	8.3	32.2	0.129		0.106		5.91	1.94	2.38	1.22
B1	22:35	10.1	31.7	0.157	0.91	0.049	0.78	3.15	0.50	1.93	1.51
C4	19:11	12.7	32.8	0.145	1.05	0.118	0.97	7.53	3.05	5.58	1.22
P1	12:15	14.0	30.6		1.09		0.83	3.59	2.89	3.70	1.61
E2	22:22	16.6	33.3	0.110	1.06	0.140	1.05	6.53	1.62	6.46	0.98
F5	7:31	20.2	34.5		1.27		0.83	5.77	-2.61	7.72	1.25
T2	21:12	17.9	33.1	0.114		0.109		3.04	-0.14	2.47	1.05
S6	8:05	23.0	34.4	0.069		0.060		4.80	-1.18	3.72	0.82
P7	20:15	23.0	34.7		0.82		0.71	7.32	3.79	12.45	1.20
Average		16.2	33.0	0.121	1.03	0.097	0.86	5.29	1.10	5.16	1.21

References

- Carpenter, J. H., The Chesapeake Bay Institute technique for the Winkler dissolved oxygen method. *Limnol. Oceanogr.* 10(1964), 141–143, 1964.
- Chari, N. V. H. K., Sarma, N. S., Pandi, S. R., and Murthy, K. N., Seasonal and spatial constraints of fluorophores in the midwestern Bay of Bengal by PARAFAC analysis of excitation emission matrix spectra. *Estuar. Coast. Shelf. S.* 100, 162–171, 2012.
- Chen, Y., Yang, G., Xia, Q., and Wu, G., Enrichment and characterization of dissolved organic matter in the surface microlayer and subsurface water of the South Yellow Sea. *Mar. Chem.* 182(Mar. 20), 1–13, 2016.
- Chowdhury, S., Trihalomethanes in drinking water: Effect of natural organic matter distribution. *Water SA* 39(1), 1–7, 2013.
- Helms, J. R., Stubbins, A., Ritchie, J. D., Minor, E. C., Kieber, D. J., and Mopper, K., Absorption spectral slopes and slope ratios as indicators of molecular weight, source, and photobleaching of chromophoric dissolved organic matter. *Limnol. Oceanogr.* 53(3), 955–969, 2008.
- Hoge, F. E., Vodacek, A., and Blough, N. V., Inherent optical properties of the ocean: retrieval of the absorption coefficient of chromophoric dissolved organic matter from fluorescence measurements. *Limnol. Oceanogr.* 38(7), 1394–1402, 1993.
- Guo, W., Yang, L., Zhai, W., Chen, W., Osburn, C. L., Huang, X., and Li, Y., Runoff - mediated seasonal oscillation in the dynamics of dissolved organic matter in different branches of a large bifurcated estuary—The Changjiang Estuary. *J. Geophys. Res. -Biogeosciences* 119 (5), 776–793, 2014.
- Kowalczuk, P., Cooper, W. J., Durako, M. J., Kahn, A. E., Gonsior, M., and Young, H., Characterization of dissolved organic matter fluorescence in the South Atlantic Bight with use

- of PARAFAC model: relationships between fluorescence and its components, absorption coefficients and organic carbon concentrations. *Mar. Chem.* 118 (1–2), 22–36, 2010.
- Massicotte, P., Asmala, E., Stedmon, C., and Markager, S., Global distribution of dissolved organic matter along the aquatic continuum: Across rivers, lakes and oceans. *Sci. Total. Environ.* 609(Dec. 31), 180–191, 2017.
- Ortega-Retuerta, E., Passow, U., Duarte, C. M., and Reche, I., Effects of ultraviolet B radiation on (not so) transparent exopolymer particles. *Biogeosciences* 6(12), 3071–3080, 2009.
- Parsons, T. R., Matia, Y., and Lalli, C. M., *A Manual of Chemical and Biological Methods for Seawater Analysis*. Pergamon Press, Oxford, 1984.
- Singh, S., D'Sa, E., and Swenson, E., Seasonal variability in CDOM absorption and fluorescence properties in the Barataria Basin, Louisiana, USA. *J. Environ. Sci.* 22(10), 1481–1490, 2010.
- Spencer, R. G., Aiken, G. R., Butler, K. D., Dornblaser, M. M., Striegl, R. G., and Hernes, P. J., Utilizing chromophoric dissolved organic matter measurements to derive export and reactivity of dissolved organic carbon exported to the Arctic Ocean: a case study of the Yukon river, Alaska. *Geophys. Res. Lett.* 36(6), 141–153, 2009.
- Stedmon, C. A., and Bro, R., Characterizing dissolved organic matter fluorescence with parallel factor analysis: a tutorial. *Limnol. Oceanogr.-methods* 6(11), 572–579, 2008.
- Stedmon, C. A., Markager, S., Tranvik, L., Kronberg, L., Slätis, T., and Martinsen, W., Photochemical production of ammonium and transformation of dissolved organic matter in the Baltic Sea. *Mar. Chem.* 104(3–4), 227–240, 2007.
- Weishaar, J. L., Aiken, G. R., Bergamaschi, B. A., Fram, M. S., Fujii, R., and Mopper, K., Evaluation of specific ultraviolet absorbance as an indicator of the chemical composition and reactivity of dissolved organic carbon. *Environ. Sci. Technol.* 37(20), 4702–4708, 2003.

Williams, C. J., Yamashita, Y., Wilson, H. F., Jaffé, R., and Xenopoulos, M. A., Unraveling the role of land use and microbial activity in shaping dissolved organic matter characteristics in stream ecosystems. *Limnol. Oceanogr.* 55(3), 1159–1171, 2010.

Zepp, R. G., Sheldon, W. M., and Moran, M. A., Dissolved organic fluorophores in southeastern US coastal waters: correction method for eliminating Rayleigh and Raman scattering peaks in excitation–emission matrices. *Mar. Chem.* 89(1), 15–36, 2004.

Zhu, W. Z., Yang, G., and Zhang, H., Photochemical behavior of dissolved and colloidal organic matter in estuarine and oceanic waters, *Sci. Total Environ.* 607–608, 214–224, 2017.